ACS APPLIED MATERIALS & INTERFACES

Research Article

www.acsami.org

Improvement of J_{sc} in a Cu_2ZnSnS_4 Solar Cell by Using a Thin Carbon Intermediate Layer at the Cu_2ZnSnS_4/Mo Interface

Fangzhou Zhou,[†,§] Fangqin Zeng,[‡,§] Xu Liu,[†] Fangyang Liu,[*,‡] Ning Song,[†] Chang Yan,[†] Aobo Pu,[†] Jongsung Park,[†] Kaiwen Sun,[†] and Xiaojing Hao[*,†]

[†]School of Photovoltaic and Renewable Energy Engineering, University of New South Wales, Sydney, New South Wales 2052, Australia

[‡]School of Metallurgy and Environment, Central South University, Changsha, Hunan 410083, China

Supporting Information

ABSTRACT: Back contact modification plays an important role in improving energy conversion efficiency of Cu_2ZnSnS_4 (CZTS) thin film solar cells. In this paper, an ultrathin carbon layer is introduced on molybdenum (Mo)-coated soda lime glass (SLG) prior to the deposition of CZTS precursor to improve the back contact and therefore enhance CZTS solar cell efficiency. By introducing this layer, the short circuit current (J_{sc}) and device conversion efficiency increase for both nonvacuum (sol–gel) and vacuum (sputtering) methods. Specifically, for the sol–gel based process, J_{sc} increases from 13.60 to 16.96 mA/cm^2 and efficiency from 4.47% to 5.52%, while for the sputtering based process, J_{sc} increases from 17.50 to 20.50 mA/cm^2 and efficiency from 4.10% to 5.20%. Furthermore, introduction of this layer does not lead to any deterioration of either open circuit voltage (V_{oc}) or fill factor (FF).

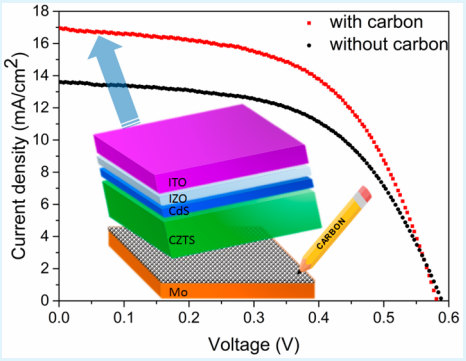

KEYWORDS: *Cu_2ZnSnS_4 (CZTS), kesterite, back contact, carbon, thin film, solar cells*

INTRODUCTION

The newly emerged kesterite $Cu_2ZnSn(S,Se)_4$ (CZTS(e)), derived from $CuIn_xGa_{(1-x)}Se_2$(CIGS), has been considered as one of the most promising absorber materials for thin film solar cell, due to its merit like earth abundant material, nontoxic composition, and good photoelectrical properties (high absorption coefficient of 10^{-4} cm^{-1} and adjustable bandgap).[1,2]

In the recent five years, this kesterite solar cell has had tremendous improvement in its efficiency, with an annual increase of ∼1%. The latest highest power conversion efficiencies of 9.1%[3] and 12.7%[4] have been achieved by IBM group for CZTS and CZTSSe solar cells, respectively.

Most of the reported high efficiency CZTS(e) devices[5−8] have been obtained from a "two-stage" process, i.e., precursor deposition followed by sulfurization/selenisation treatment. This "two-stage" process is required since high S(e) partial pressures are needed whenever CZTS(e) is processed at high temperature (500−600 °C), whereas the actual film deposition cannot typically be carried out under the same conditions.[8] Currently, one of the bottlenecks for the development of CZTS solar cells is the nonoptimized back contact interface between Mo and CZTS. During the sulfurization process, CZTS will react with Mo back contact and decompose into secondary phases, i.e., ZnS, SnS, and CuS, and MoS_2 forms simultaneously.[8] SnS would escape from the back contact region and leave voids behind, due to its high volatility. The voids block the carrier transportation and thereby deteriorate device performance.[9] In addition, MoS_2 too thick can make the back contact of CZTS and Mo nonohmic, hindering the hole extraction from absorber. Therefore, the back contact issue increases the series resistance (R_s) and reduces fill factor (FF) and short circuit current (J_{sc}).

In order to relieve this issue, several methods have been reported. For instance, TiN[10] or TiB_2[11] has been reported as the sulfur isolation layer for Mo to inhibit the formation of MoS_2. In addition, ZnO[12] and Ag[13] have been employed at back contact to relieve/slow down the process of Mo sulfurization. All these inserting materials suppress somewhat the decomposition and void formation at back contact. However, even though all these materials boost efficiency, they still have some side effects on performance. Herein, we present a convenient way to resolve this problem by simply inserting an ultrathin carbon layer between CZTS and Mo. Carbon is an inert material to sulfur and possesses superior conductivity. When an ultrathin carbon layer is inserted between CZTS and Mo, the carbon does not block the formation of MoS_2, which retains the advantages of high work function and qusai-ohmic contact,[11] and carbon reconnects CZTS absorber and MoS_2 back contact through the voids. Our result shows that an ultrathin carbon layer can readily boost J_{sc} and efficiency of CZTS solar cells, without deterioration of open circuit voltage (V_{oc}) or FF.

Received: June 25, 2015
Accepted: September 29, 2015
Published: September 29, 2015

DOI: 10.1021/acsami.5b05652
ACS Appl. Mater. Interfaces 2015, 7, 22868−22873

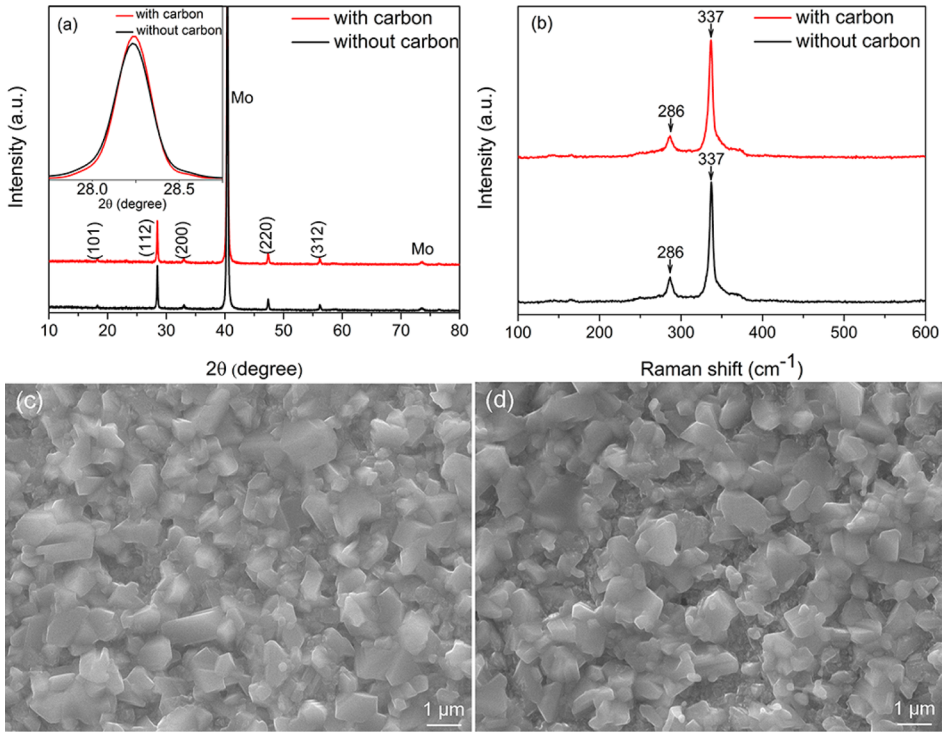

Figure 1. (a) XRD pattern (inset: the comparison of (112) plane); (b) Raman spectra; top-view SEM image of CZTS absorber: (c) without carbon layer and (d) with carbon layer.

EXPERIMENTAL SECTION

Preparation of Carbon on Mo Coated Soda Lime Glass Substrates. For some samples, prior to CZTS deposition, a thin carbon layer (~25 nm) was grown on a Mo-coated soda lime glass (SLG) substrate by the evaporation system (Emitech sputter coater K575x with Quorum Tech CA7625 carbon coating accessory, graphite rod as carbon source).

Preparation of CZTS. To evaluate the effectiveness of carbon intermediate layer, CZTS films made from two different fabrication methods have been used in this work.

CZTS via Sol–Gel Based Method. The precursor solution was prepared by dissolving 10.65 g of copper(II) acetate monohydrate ($Cu(CH_3COO)_2{\cdot}H_2O$, 99%) (53.30 mmol), 7.32 g of zinc acetate dihydrate ($Zn(CH_3COO)_2\ 2H_2O$, 99%) (33.40 mmol), 6.02 g of tin(II) chloride ($SnCl_2$, 98%) (26.70 mmol, AR), and 16.16 g of thiourea ($SC(NH_2)_2$, 99%) (210 mmol) into 100 mL of 2-methoxyethanol ($(HOCH_2CH_2)_3N$, 98%) and stirring at 50 °C for 1 h to get a light yellow solution. All chemicals and solvents were used as purchased from Aladdin without any further purification. The precursor solution was then spin-coated on Mo-coated SLG substrates at 800 rpm for 10 s and then 3000 rpm for 20 s, followed by drying at 300 °C for 5 min on a hot plate in air. This coating step was repeated 15 times to get a CZTS precursor film with a desired thickness. After that, the prepared precursor films were sulfurized at 540 °C in a sulfur/N_2 atmosphere for 40 min with controlled sulfur partial pressure, to form the CZTS absorber.

CZTS via Sputtering Based Method. A magnetron sputtering system (AJA International, Inc., model ATC-2200) was used to cosputter Cu–ZnS–SnS precursors on Mo-coated SLG substrates. These precursors were then subject to sulfurization using a Rapid Thermal Processor (AS-One 100) at 560 °C for 1 min in a sulfur containing atmosphere.

Devices Fabrication. The solar cell devices were completed by a chemical bath deposited 70 nm CdS buffer, followed by RF magnetron sputtered 50 nm intrinsic ZnO, and DC magnetron sputtered 200 nm ITO window layer sequentially. Finally, Al was thermally evaporated on the ITO layer to form top contact fingers via a shadow mask. Each device had a total area of approximately 0.45 cm^2 (total area) defined by mechanical scribing.

Characterization. The surface morphology of the carbon layer was measured by the scanning probe microscope (SPM) (Bruker Dimension ICON SPM). The X-ray diffraction (XRD) patterns and Raman spectra were measured by Rigaku D/Max2500 and Jobin-Yvon LabRAM HR-800 (514 nm excitation wavelength), respectively. The surface morphology of the thin films was characterized by a scanning electron microscope (SEM) (MIRA3 TESCAN). An energy dispersive spectrometer (EDS, EDAX-GENSIS60S in MIRA3 TESCAN) was used to check the elemental. A FEI Tecnai G2 equipped with an energy dispersive spectroscopy detector was used for the transmission electron microscopy (TEM) and element distribution analyses. Current density–voltage (J–V) characterization for the solar cells was performed using an Xe based light source solar simulator (Newport, 91160 and KEITHLEY 2400) to provide simulated 1 sun AM 1.5G illumination which was calibrated with a standard Si reference cell, traceable to the National Renewable Energy Laboratory. The external quantum efficiency (EQE) was measured using a chopped monochromatic beam and lock-in amplifier, with calibration by a Silicon diode measurement (QEX10 spectral response system from PV measurements, Inc.).

RESULTS AND DISCUSSION

To assess the effect of carbon on CZTS absorber quality, the quality of deposited carbon layer needs to be checked first. The average roughness and morphology are hints for whether the obtained carbon layer is uniform or not. If the carbon layer is continuous and uniform with good coverage, the average roughness value should have negligible change after carbon deposition and the morphology should maintain the same features. The two-dimensional SPM images of Mo-coated SLG substrate before and after ultrathin carbon layer deposition are shown in Figure S1. In the case of Mo surface without carbon coating (Figure S1a), the average roughness value of the surface is 8.44 nm. In the case of the Mo surface with carbon coating

DOI: 10.1021/acsami.5b05652
ACS Appl. Mater. Interfaces 2015, 7, 22868–22873

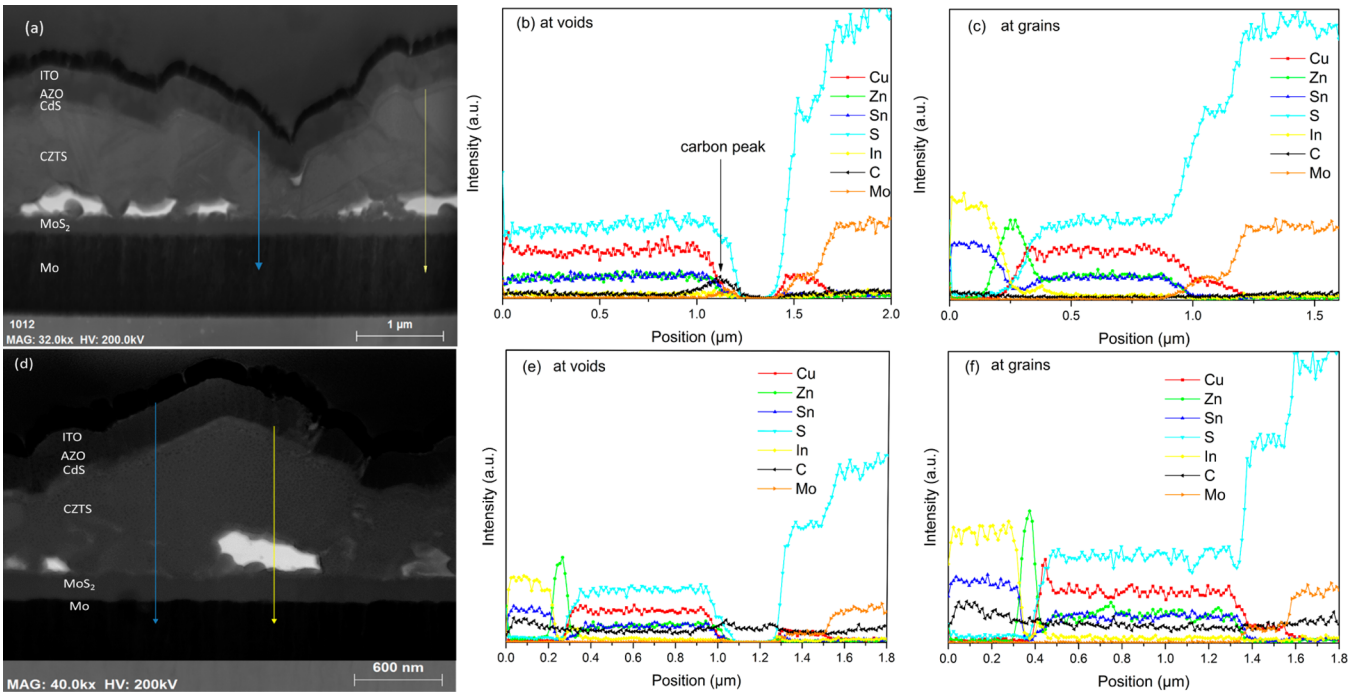

Figure 2. (a) Cross-sectional TEM image of the CZTS based device with the carbon layer; EDS line scan for the compositional vertical distribution of the CZTS based device with the carbon layer: (b) on void region and (c) on grain region. (d) Cross-sectional TEM image of the CZTS based device without the carbon layer; EDS line scan for the compositional vertical distribution of the CZTS based device without the carbon layer: (e) on void region and (f) on grain region (CZTS absorber in both devices was fabricated by the sol−gel method).

(in Figure S1b), the average roughness value of the surface is still 8.44 nm and the microstructure remains. The similar average roughness value and morphology indicate that the ultrathin carbon is uniformly and continuously deposited on the top of Mo without modifying the microstructure of the substrate.

XRD, Raman, and SEM were applied in the evaluation of the effects of carbon layer on the overlying CZTS absorber's crystallinity, phase constitution, and morphology (by sol−gel method). As shown from the XRD patterns in Figure 1a, the absorbers with and without carbon layer both present kesterite structure of CZTS, and no peaks assigned to secondary phases such as CuS_x, SnS, and SnS_2 can be observed.[14] The inset of Figure 1a shows a comparison of the enlarged (112) peaks of the CZTS absorbers with and without carbon layer. No peak broadening or shifting can be identified when the carbon layer is introduced, suggesting that the introduction of the carbon layer has little impact on the crystallinity of CZTS absorber. However, the presence of ZnS and Cu_2SnS_3 (CTS) impurities cannot be ruled out because of high similarity of their XRD patterns compared to those of CZTS.[15] To further confirm the phase constitution of the CZTS films with or without the carbon intermediate layer, Raman characterization was carried out. As demonstrated in Figure 1b, for the CZTS thin film with the carbon intermediate layer, the major peaks appear at 286 and 337 cm^{-1}, consistent with those of the CZTS thin film without the carbon layer.[14] There is no observation of secondary phases like ZnS(355 cm^{-1})[14] or CTS. The complementary studies based on XRD and Raman spectroscopy confirm that the single phase CZTS thin films were achieved in the cases with and without a carbon intermediate layer. Also, no obvious diffraction peak attributed to graphite nitridation or carbon disulfide was observed. Moreover, the insertion of carbon prior to the CZTS deposition has no effects on the phase composition and crystallinity of the synthesized CZTS films.

Large grain is favorable for device performance since the grain boundary tends to become sinks for both chemical impurities and structural defects, normally creates deep levels that act as a recombination center, and reduces the majority mobility of CZTS.[16,17] Figure 1c,d shows the top-view SEM images of sulfurized CZTS thin films without and with a carbon intermediate layer, respectively. When carbon layer is introduced, the surface of the thin film is kept compactly packed as that without the carbon layer, and the average grain sizes are quiet analogous, around 1 μm for both samples. Except for the crystal structure and surface morphology, the chemical composition of the CZTS thin films is another important factor that affects the performance of the CZTS devices.[18] The composition (here using atomic ratios) of the CZTS absorber (by sol−gel method) from the EDS measurement without the carbon layer is Cu/(Zn + Sn) ~ 0.76 and Zn/Sn ~ 1.05, while that with the carbon layer is Cu/(Zn + Sn) ~ 0.78 and Zn/Sn ~ 1.04, revealing almost no change in chemical composition with the introduction of the carbon intermediate layer. The similar morphology and chemical composition of the absorber with and without the carbon layer suggest that the insertion of the carbon intermediate layer does not cause side effects, and Cu-poor, Zn-rich, and dense CZTS absorbers can be formed.

Cross-sectional TEM image and EDS line scan images of the fabricated CZTS solar cell (by sol−gel method) with and without the 25 nm carbon intermediate layer are displayed in Figure 2. As shown in Figure 2a, voids and a 200 nm MoS_2 interfacial layer are evident between the CZTS absorber layer and Mo back contact for the device with the carbon layer. The carbon intermediate layer does not inhibit generation of voids or MoS_2 during the sulfurization process. The vertical element

DOI: 10.1021/acsami.5b05652
ACS Appl. Mater. Interfaces 2015, 7, 22868−22873

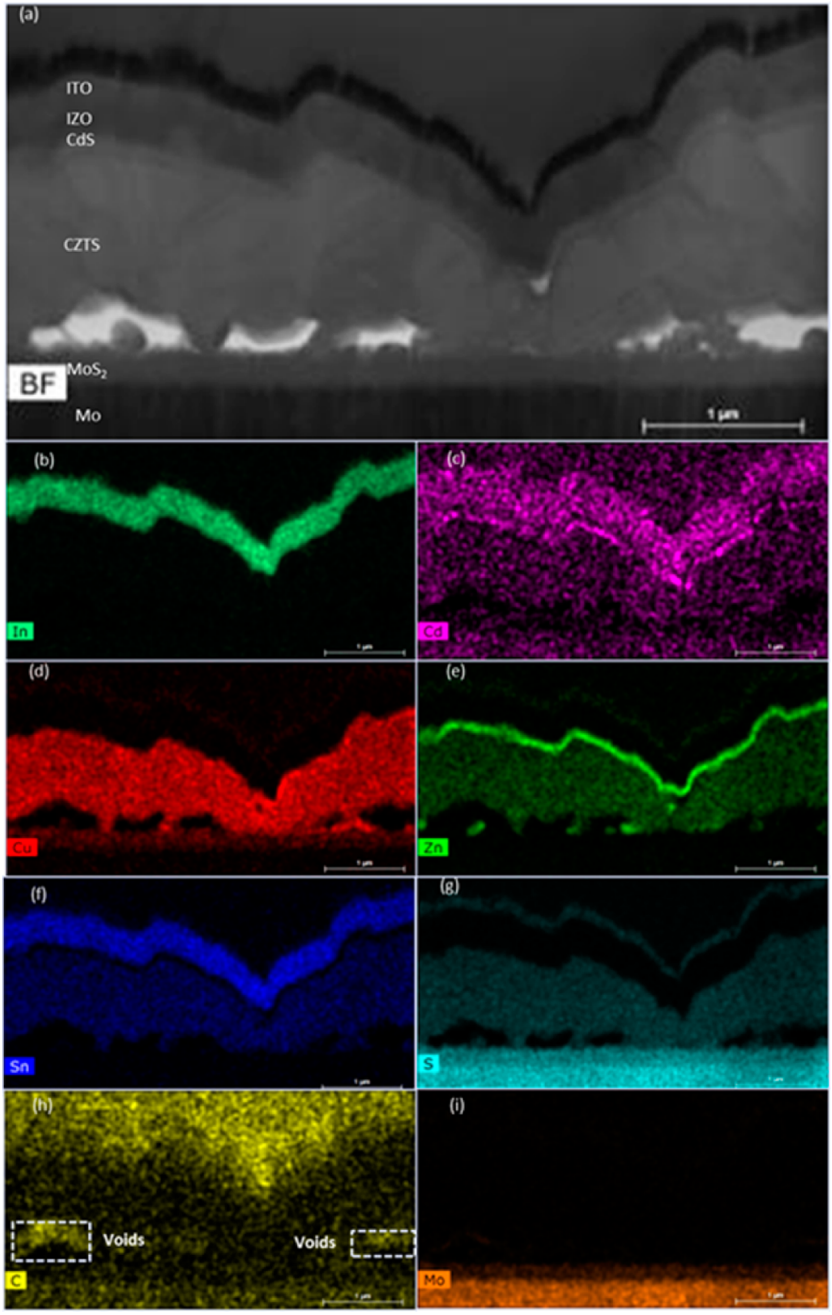

Figure 3. (a) Cross-sectional TEM image of the CZTS based device and (b–i) the EDS mapping for the compositional distribution ((b) In, (c) Cd, (d) Cu, (e) Zn, (f) Sn, (g) S, (h) C, and (i) Mo) in the whole area of (a).

distribution (along film growth direction) is characterized by EDS line scan within the TEM cross over CZTS absorber (EDS line scan spans from the CZTS absorber to Mo in Figure 2b and from ITO to Mo in Figure 2c,e,f). The arrows in Figure 2a mark the region detected by the EDS line scan: yellow one on void area with composition profile shown in Figure 2b and blue one on nonvoid area with composition profile shown in Figure 2c. In Figure 2b, the EDS signal from carbon is at a very low level on the CZTS absorber bulk region but increases considerably and forms a peak at the void region. To clarify the exact location of carbon on the void region, it is worth comparing the carbon vertical distribution with other element distributions. By comparing the distribution of sulfur, it is noticeable that the concentration of carbon rises from 1.13 μm while that of sulfur plunges from 1.10 μm and reaches the lowest point at 1.25 μm, which indicates that the void forms from around 1.10 μm, and therefore, carbon mainly sticks on the inner wall of voids in the absorber. Due to the carbon contained precursor solution used in the sol–gel based method, carbon on the inner wall of voids could be from the carbon intermediate layer or carbon residual from the precursor solution. To further investigate the origin of the carbon on the inner wall of voids, EDS line scans on the CZTS solar cell without the carbon intermediate layer were carried out. Similar to Figure 2a, arrows in Figure 2d mark the regions of EDS detection. Composition profile of the yellow arrow on the void area is shown in Figure 2e, and the composition profile of the blue one on the nonvoid area is shown in Figure 2f. In Figure

DOI: 10.1021/acsami.5b05652
ACS Appl. Mater. Interfaces 2015, 7, 22868–22873

2e, the carbon concentration is uniform showing no difference between absorber bulk and void regions. By comparing the vertical carbon distribution at the void region for CZTS solar cells with and without the carbon intermediate layer, the difference suggests that carbon sticking on the inner wall of voids should come from the deposited carbon intermediate layer. During the sulfurization, the carbon aggregates at the inner wall of voids. Thus, this good conducting layer may reconnect the CZTS and MoS_2 at the void area and thereby reduce the contact resistance. In the case of nonvoid regions (as shown in Figure 2c,f), carbon is distributed homogeneously along the arrow. In terms of TEM topology and EDS line scan, the vertical element distribution of CZTS and the thickness of each layer are similar for both CZTS solar cells with or without the carbon intermediate layer, and the only difference is the carbon distribution at the void region.

In order to confirm that the carbon aggregation phenomenon is universal to both the vacuum based and nonvacuum based method, we applied a cross-sectional TEM and EDS line scan on the CZTS solar cell with absorber fabricated by the sputter method with and without a 25 nm carbon intermediate layer. TEM images and EDS line scan graphs are shown in Figure S3. Similar to Figure 2, voids and MoS_2 interfacial layer are shown between the CZTS absorber and Mo back contact. The vertical element distribution (along film growth direction) spans from ITO to Mo back contact. The arrows in Figure S3a mark the region detected by the EDS line scan, with the yellow one on the void area with a composition profile shown in Figure S3b, and the blue one on the nonvoid area with the composition profile shown in Figure S3c. The arrows in Figure S3d mark the region detected by the EDS line scan, with the yellow one on the void area with the composition profile shown in Figure S3e, and the blue one on the nonvoid area with the composition profile shown in Figure S3f. It is notable that the concentration of carbon peaks at the void region in Figure S3b, but in Figure S3c,e,f, the EDS signal from carbon stabilizes at a very low level along the arrow. As no carbon-containing solution is involved in the sputter based method, the carbon in Figure S3b is obviously attributed to the carbon intermediate layer.

In addition, we applied EDS mapping by TEM so as to further confirm the observation of the carbon distribution. Figure 3a shows the TEM images, and Figure 3b–i shows related EDS mappings of the CZTS device (by the sol–gel method) with a carbon intermediate layer. It is demonstrated that the elements (Cu, Zn, Sn, S) of CZTS in the absorber bulk are distributed uniformly, but from the EDS mapping of carbon in Figure 3h, the aggregation of carbon at the inner wall of voids is evident, supporting the observation in Figure 2. In addition, the bigger size of voids, the more obvious the carbon aggregation phenomenon can be observed.

Figure 4 illustrates the J–V and EQE characteristics of the CZTS devices (by the sol–gel based method) with and without a carbon intermediate layer between CZTS absorbers and Mo substrates. The conversion efficiency rises from 4.47% to 5.52% when utilizing a carbon layer. This efficiency enhancement mainly results from a significant boost in J_{sc} (from 13.60 to 16.96 mA/cm^2). We speculate that the 25% increase in J_{sc} can be reasonably attributed to the aggregation of carbon on the inner walls of voids reconnecting the CZTS and back contact. Meanwhile, there is no deterioration of either V_{oc} or FF for devices with a carbon intermediate layer. The EQE spectra reveal that the J_{sc} difference between CZTS devices with and without a carbon intermediate layer is mainly due to the EQE

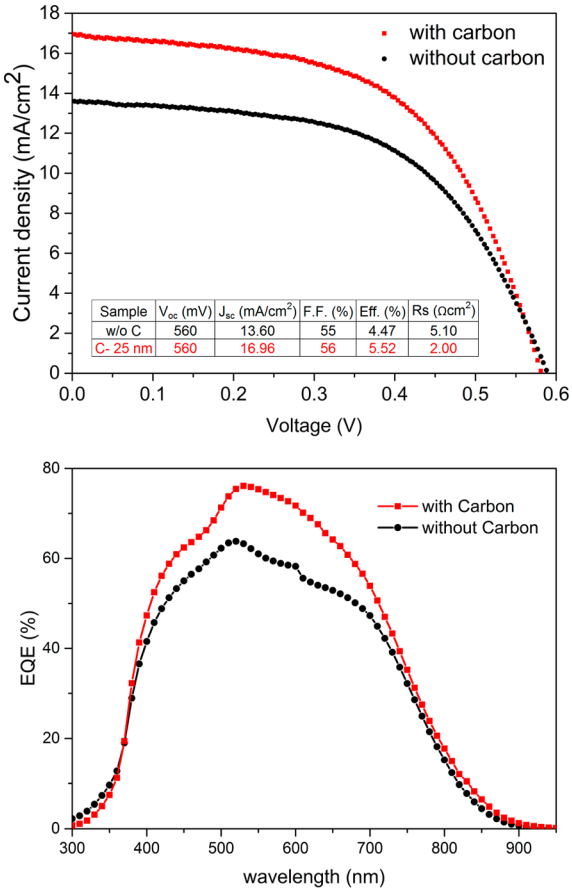

Figure 4. Illuminated J–V curves and EQE curves of CZTS solar cells (solution based, annealed at 580 °C) with and without carbon layer.

enhancement in the whole visible region, which may be explained by the reduced R_s (5.10 Ωcm^2 without carbon and 2.00 Ωcm^2 with carbon). Without the carbon intermediate layer, the large number of voids forming at the back contact region limit the free-carrier transportation, leading to higher R_s and thereby lower J_{sc}. With the introduction of the carbon intermediate layer, the carbon aggregation at the inner wall of voids connects the CZTS and back contact, which can reduce the contact resistance and thereby reduce R_s, facilitating the photogenerated current flow.

It is also worthwhile to further investigate the compatibility and effectiveness of the carbon intermediate layer concerning different CZTS syntheses methods. Therefore, we applied the carbon layer on the sputter based CZTS fabrication process. The J–V and EQE characteristic of the CZTS devices with and without the carbon intermediate layer by the sputter based method is shown in Figure S2. As expected, a significant boost in J_{sc} has been observed. With the carbon layer, the efficiency is improved from 4.10% to 5.20%, mainly attributed to an enhanced J_{sc} from 17.50 to 20.50 mA/cm^2 (increases by 17%). In addition, the V_{oc} and FF also increased slightly, from 560 to 580 mV and from 40% to 42%, respectively. This experiment proves that the carbon intermediate layer is applicative for both the vacuum based method and the nonvacuum based method. Compared to other intermediate layer materials (TiN and ZnO may lead to high R_s and reduce FF;[8,12] TiB_2 degrades crystal quality;[11] Ag is relatively expensive), not only does carbon have advantages such as low cost, high accessibility, and nontoxicity, but also, no side effect is applied on V_{oc} and FF.

DOI: 10.1021/acsami.5b05652
ACS Appl. Mater. Interfaces 2015, 7, 22868–22873

CONCLUSIONS

In summary, we develop an easy and cheap way to handle the back contact problem by inserting an ultrathin carbon intermediate layer between CZTS and Mo. We show that the utilization of this ultrathin carbon layer can readily boost the efficiency of the CZTS solar cell, especially on J_{sc}. This is due to the aggregation of carbon at the inner wall of voids and reconnection of CZTS with back contact. Comprehensive analysis of CZTS thin films with and without the carbon layer from XRD, Raman, and SEM (with EDS) indicates that introduction of the ultrathin carbon intermediate layer has no negative effect on CZTS absorber structural quality and thereby no associated negative effect on cell performance. Through the TEM and EDS line scan, the carbon intermediate layer aggregates at the inner wall of voids and thus reduces the R_s and boosts J_{sc}. This simple strategy improves the J_{sc} by 25% by the sol−gel based method and 17% by the sputter based method. It is effective and can be widely utilized in both vacuum and nonvacuum deposited CZTS devices.

ASSOCIATED CONTENT

Supporting Information

The Supporting Information is available free of charge on the ACS Publications website at DOI: 10.1021/acsami.5b05652.

SPM images of Mo before and after carbon deposition. Cross-sectional TEM image and EDS line scan for the compositional vertical distribution of the CZTS based device with and without the carbon layer (CZTS absorber in both devices was fabricated by the sputtering method). (PDF)

AUTHOR INFORMATION

Corresponding Authors

*E-mail: fangyang.liu@unsw.edu.au.

*E-mail: xj.hao@unsw.edu.au.

Author Contributions

§F. Zhou and F. Zeng contributed equally.

Notes

The authors declare no competing financial interest.

ACKNOWLEDGMENTS

This work has been financially supported by the Australian Government through the Australian Renewable Energy Agency (ARENA) and Australian Research Council (ARC) and Guodian New Energy Technology Research Institute, China Guodian Corporation. Responsibility for the views, information or advice expressed herein is not accepted by the Australian Government. The authors acknowledge the facilities and the scientific and technical assistance of the Australian Microscopy & Microanalysis Research Facility at the Electron Microscope Unit, The University of New South Wales (UNSW). The authors also acknowledge Dr. Jialiang Huang for his great help with the TEM measurement.

REFERENCES

(1) Mitzi, D. B.; Gunawan, O.; Todorov, T. K.; Wang, K.; Guha, S. The Path Towards a High-performance Solution-processed Kesterite Solar Cell. *Sol. Energy Mater. Sol. Cells* **2011**, *95*, 1421−1436.

(2) Mitzi, D. B.; Gunawan, O.; Todorov, T. K.; Barkhouse, D. A. R. Prospects and Performance Limitations for Cu−Zn−Sn−S−Se Photovoltaic Technology. *Philos. Trans. R. Soc., A* **2013**, *371*, 20110432.

(3) Green, M. A.; Emery, K.; Hishikawa, Y.; Warta, W.; Dunlop, E. D. Solar Cell Efficiency Tables (Version 46). *Prog. Photovoltaics* **2015**, *23*, 805−812.

(4) Wang, W.; Winkler, M. T.; Gunawan, O.; Gokmen, T.; Todorov, T. K.; Zhu, Y.; Mitzi, D. B. Device Characteristics of CZTSSe Thin-Film Solar Cells with 12.6% Efficiency. *Adv. Energy Mater.* **2014**, *4*, 1301465.

(5) Todorov, T. K.; Tang, J.; Bag, S.; Gunawan, O.; Gokmen, T.; Zhu, Y.; Mitzi, D. B. Beyond 11% Efficiency: Characteristics of State-of-the-Art $Cu_2ZnSn(S,Se)_4$ Solar Cells. *Adv. Energy Mater.* **2013**, *3*, 34−38.

(6) Shin, B.; Gunawan, O.; Zhu, Y.; Bojarczuk, N. A.; Chey, S. J.; Guha, S. Thin Film Solar Cell with 8.4% Power Conversion Efficiency Using an Earth-Abundant Cu_2ZnSnS_4 Absorber. *Prog. Photovoltaics* **2013**, *21*, 72−76.

(7) Repins, I.; Beall, C.; Vora, N.; DeHart, C.; Kuciauskas, D.; Dippo, P.; To, B.; Mann, J.; Hsu, W.-C.; Goodrich, A.; Noufi, R. Co-Evaporated $Cu_2ZnSnSe_4$ Films and Devices. *Sol. Energy Mater. Sol. Cells* **2012**, *101*, 154−159.

(8) Scragg, J. J.; Kubart, T.; Wätjen, J. T.; Ericson, T.; Linnarsson, M. K.; Platzer-Björkman, C. Effects of Back Contact Instability on Cu_2ZnSnS_4 Devices and Processes. *Chem. Mater.* **2013**, *25*, 3162−3171.

(9) Li, W.; Chen, J.; Cui, H.; Liu, F.; Hao, X. Inhibiting MoS_2 Formation by Introducing a ZnO Intermediate Layer for Cu_2ZnSnS_4 Solar Cells. *Mater. Lett.* **2014**, *130*, 87−90.

(10) Shin, B.; Zhu, Y.; Bojarczuk, N. A.; Jay Chey, S.; Guha, S. Control of an Interfacial $MoSe_2$ Layer in $Cu_2ZnSnSe_4$ Thin Film Solar Cells: 8.9% Power Conversion Efficiency with a TiN Diffusion Barrier. *Appl. Phys. Lett.* **2012**, *101*, 053903.

(11) Liu, F.; Sun, K.; Li, W.; Yan, C.; Cui, H.; Jiang, L.; Hao, X.; Green, M. A. Enhancing the Cu_2ZnSnS_4 Solar Cell Efficiency by Back Contact Modification: Inserting a Thin TiB_2 Intermediate Layer at Cu_2ZnSnS_4/Mo Interface. *Appl. Phys. Lett.* **2014**, *104*, 051105.

(12) Lopez-Marino, S.; Placidi, M.; Perez-Tomas, A.; Llobet, J.; Izquierdo-Roca, V.; Fontane, X.; Fairbrother, A.; Espindola-Rodriguez, M.; Sylla, D.; Perez-Rodriguez, A.; Saucedo, E. Inhibiting the Absorber/Mo-back Contact Decomposition Reaction in $Cu_2ZnSnSe_4$ Solar Cells: the Role of a ZnO Intermediate Nanolayer. *J. Mater. Chem. A* **2013**, *1*, 8338−8343.

(13) Cui, H.; Liu, X.; Liu, F.; Hao, X.; Song, N.; Yan, C. Boosting Cu_2ZnSnS_4 Solar Cells Efficiency by a Thin Ag Intermediate Layer Between Absorber and Back Contact. *Appl. Phys. Lett.* **2014**, *104*, 041115.

(14) Fernandes, P. A.; Salomé, P. M. P.; da Cunha, A. F. Growth and Raman Scattering Characterization of Cu_2ZnSnS_4 Thin Films. *Thin Solid Films* **2009**, *517*, 2519−2523.

(15) Riha, S. C.; Parkinson, B. A.; Prieto, A. L. Solution-Based Synthesis and Characterization of Cu_2ZnSnS_4 Nanocrystals. *J. Am. Chem. Soc.* **2009**, *131*, 12054−12055.

(16) Seto, J. Y. W. The Electrical Properties of Polycrystalline Silicon Films. *J. Appl. Phys.* **1975**, *46*, 5247−5254.

(17) Yan, Y.; Al-Jassim, M. M.; Jones, K. M. Structure and Effects of Double-Positioning Twin Boundaries in CdTe. *J. Appl. Phys.* **2003**, *94*, 2976−2979.

(18) Katagiri, H.; Jimbo, K.; Tahara, M.; Araki, H.; Oishi, K. The Influence of the Composition Ratio on CZTS-Based Thin Film Solar Cells. *MRS Online Proc. Libr.* **2009**, *1165*; DOI: 10.1557/PROC-1165-M04-01

DOI: 10.1021/acsami.5b05652
ACS Appl. Mater. Interfaces 2015, 7, 22868−22873